

# Strong correlation and massive spectral-weight redistribution induced spin density wave in $\alpha$ -Fe<sub>1.06</sub>Te

Y. Zhang,<sup>1</sup> F. Chen,<sup>1</sup> C. He,<sup>1</sup> L. X. Yang,<sup>1</sup> B. P. Xie,<sup>1</sup> Y. L. Xie,<sup>2</sup> X. H. Chen,<sup>2</sup> Minghu Fang,<sup>3</sup> M. Arita,<sup>4</sup> K. Shimada,<sup>4</sup> H. Namatame,<sup>4</sup> M. Taniguchi,<sup>4</sup> J. P. Hu,<sup>5</sup> and D. L. Feng<sup>1,\*</sup>

<sup>1</sup>*Department of Physics, Surface Physics Laboratory (National Key Laboratory), and Advanced Materials Laboratory, Fudan University, Shanghai 200433, People's Republic of China*

<sup>2</sup>*Department of Physics, University of Science and Technology of China, Hefei, Anhui 230027, People's Republic of China*

<sup>3</sup>*Department of Physics, Zhejiang University, Hangzhou 310027, China*

<sup>4</sup>*Hiroshima Synchrotron Radiation Center and Graduate School of Science, Hiroshima University, Hiroshima 739-8526, Japan.*

<sup>5</sup>*Department of Physics, Purdue University, West Lafayette, Indiana 47907, USA*

(Dated: June 12, 2018)

The electronic structure of  $\alpha$ -Fe<sub>1.06</sub>Te is studied with angle-resolved photoemission spectroscopy. We show that there is substantial spectral weight around  $\Gamma$  and  $X$ , and lineshapes are intrinsically incoherent in the paramagnetic state. The magnetic transition is characterized by a massive spectral-weight transfer over an energy range as large as the band width, which even exhibits a hysteresis loop that marks the strong first order transition. Coherent quasiparticles emerge in the magnetically ordered state due to decreased spin fluctuations, which account for the change of transport properties from insulating behavior to metallic behavior. Our observation demonstrates that Fe<sub>1.06</sub>Te distinguishes itself from other iron-based systems with more local characters and much stronger interactions among different degrees of freedom, and how a spin density wave is formed in the presence of strong correlation.

The discovery of iron-based high-temperature superconductors (Fe-HTSCs) has generated great interests [1]. So far, two classes of Fe-HTSC have been discovered. They are iron pnictides, *e.g.*, SmO<sub>1-x</sub>F<sub>x</sub>FeAs or Ba<sub>1-x</sub>K<sub>x</sub>Fe<sub>2</sub>As<sub>2</sub> [2, 3], and iron chalcogenides, *e.g.*, Fe<sub>1+y</sub>Te<sub>1-x</sub>Se<sub>x</sub> [4]. Although, both classes of materials share many common aspects, such as similarly high maximal superconducting transition temperature ( $T_c$ ) (Fe<sub>1+y</sub>Se possesses a  $T_c$  of 37 K under hydrostatic pressure of 7 GPa [5]) and similar band structures from density-functional theory (DFT) calculations [6, 7]. However, their parent compounds exhibit quite different spin density wave (SDW) states. A collinear commensurate antiferromagnetic order has been identified for the pnictides [8, 9], while a bicollinear and 45-degree rotated antiferromagnetic order was identified for Fe<sub>1+y</sub>Te [10, 11]. Furthermore, the transport properties of Fe<sub>1+y</sub>Te respond abruptly to the first order magnetic/structural transition. In the paramagnetic state, it shows insulator-like resistivity [Fig. 1(e)], and optical conductivity without a Drude peak, while the resistivity becomes metallic-like, and a Drude peak emerges in the SDW state [12, 13].

Like the cuprates, the nature of magnetic order and spin fluctuations in Fe-HTSC are most likely crucial for its superconductivity. Yet the origin of the magnetic ordering in iron pnictides/chalcogenides is still under heated debate. For the iron pnictides, previous studies have shown that the large reconstruction of the band structure dominates the savings of electronic energy, and would be

responsible for the SDW [14–16], while there are also suggestions that the SDW might be dominated by Fermi surface nesting [17]. For the iron chalcogenides, a connection between the electronic structure and the bicollinear magnetic structure has not been established, except that Fermi surface nesting has been ruled out [12, 18]. Many fundamental questions are yet to be addressed for iron chalcogenides: is there any connection between the electronic structure and magnetic ordering; and why is it different from the iron pnictides; what is responsible for the anomalous transport behaviors in iron chalcogenides? The answers of these questions will help build a general picture of iron-based superconductors.

In this Letter, we study the electronic structure of a prototypical parent iron chalcogenide,  $\alpha$ -Fe<sub>1.06</sub>Te, by angle-resolved photoemission spectroscopy (ARPES). We found that it is profoundly different from those of iron pnictides. The electronic structure of Fe<sub>1.06</sub>Te is dominated by strong correlation, which induces incoherent spectra over extended momentum region in the paramagnetic state. A large square shape of spectral weight unexpectedly appear around  $\Gamma$  and extend to  $X$  near the Fermi energy ( $E_F$ ). In the SDW state, with the spectral weight redistribution over a large energy scale of 0.7 eV, sharp quasiparticle peaks emerge near  $E_F$ , indicating reduced spin fluctuations. Through detailed temperature-dependence studies, we prove that the massive redistribution of the spectral weight is responsible for the magnetic transition, unveiling a unique manifestation of SDW on electronic structure in the presence of strong correlation.

$\alpha$ -Fe<sub>1.06</sub>Te single crystals were synthesized following the method in Ref. [19]. Magnetic susceptibility measurements show that the SDW transition occurs at  $T_s = 70$  K,

\*Electronic address: dlffeng@fudan.edu.cn

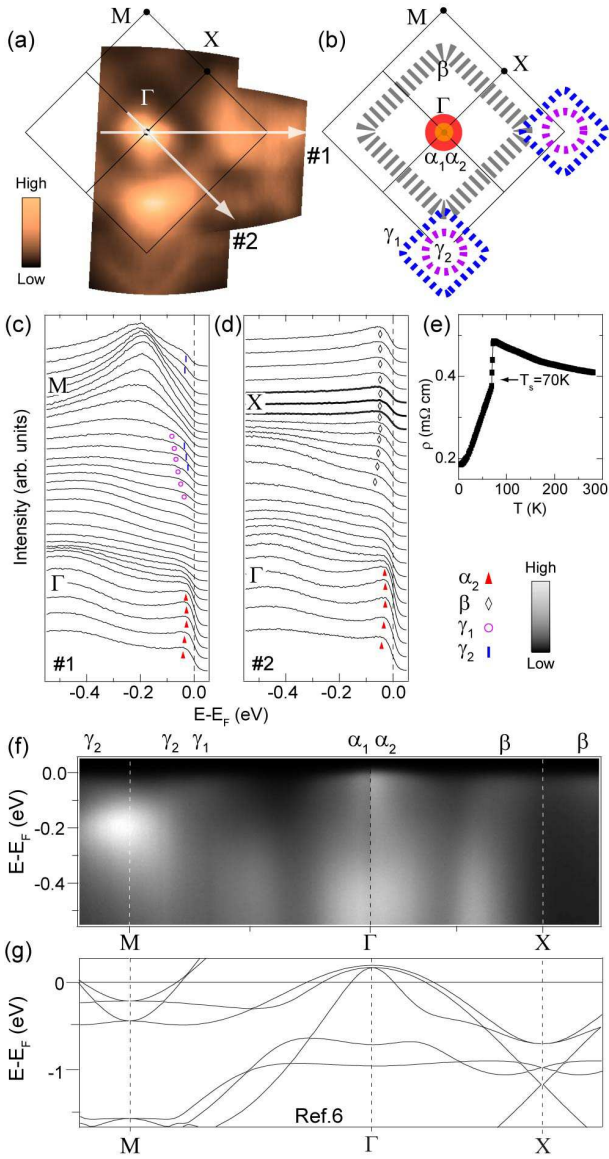


FIG. 1: (Color online) Paramagnetic state electronic structure of Fe<sub>1.06</sub>Te measured at 135 K. (a) Photoemission intensity distribution integrated over the energy window of  $[E_F - 15 \text{ meV}, E_F + 15 \text{ meV}]$ . (b) The spectral-weight distribution around  $E_F$ , which are labeled by the filled orange circle ( $\alpha_1$ ), the red circle ( $\alpha_2$ ), the dashed black square ( $\beta$ ), the dashed blue squares ( $\gamma_1$ ), and dashed purple squares ( $\gamma_2$ ). (c) and (d) The energy distribution curves (EDCs) along cut #1 and #2 respectively. (e) The temperature dependence of the resistivity of Fe<sub>1.06</sub>Te. (f) The photoemission intensities along the  $M-\Gamma-X$  high symmetry lines, and (g) the corresponding band structure based on DFT calculations. [6].

accompanied by a structural transition, which is consistent with the neutron and transport reports [11, 12]. ARPES data were taken with circularly polarized 24 eV photon at the Beamline 9 of Hiroshima synchrotron radiation center (HiSOR) with a Scienta R4000 electron analyzer. The energy resolution is 10 meV, and angular

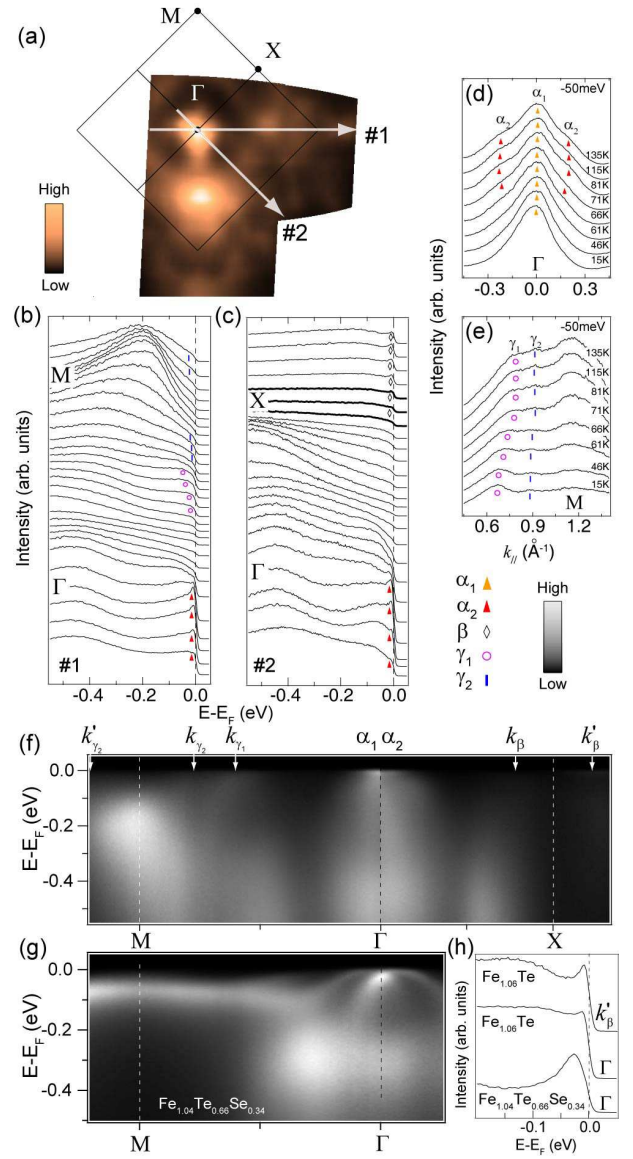


FIG. 2: (Color online) SDW state electronic structure of Fe<sub>1.06</sub>Te measured at 15 K. (a) Photoemission intensity distribution integrated over the energy window of  $[E_F - 15 \text{ meV}, E_F + 15 \text{ meV}]$ . (b) and (c) The EDCs along cut #1 and cut #2 respectively. (d) and (e) are momentum distribution curves (MDCs) at  $-50 \text{ meV}$  around  $\Gamma$  and  $M$  at different temperatures respectively. (f) The photoemission intensities along the  $M-\Gamma-X$  high symmetry lines. Various Fermi crossings are denoted by the short arrows. (g) The photoemission intensity of Fe<sub>1.04</sub>(Te<sub>0.66</sub>Se<sub>0.34</sub>) along  $M-\Gamma$ . (h) The EDCs taken at 15 K for Fe<sub>1.04</sub>(Te<sub>0.66</sub>Se<sub>0.34</sub>) at  $\Gamma$ , and for Fe<sub>1.06</sub>Te at  $\Gamma$  and  $k'_\beta$ .

resolution is  $0.3^\circ$ . The sample was cleaved *in situ*, and measured under ultrahigh vacuum of  $3 \times 10^{-11}$  torr. Aging effects are strictly monitored during the experiments.

The electronic structure of Fe<sub>1.06</sub>Te in the paramagnetic state is shown in Fig. 1. The spectra are characterized by broad incoherent feature, while the quasipar-

ticle weight is negligibly small. Thus, Fermi crossings are not well-defined, analogous to the pseudogap in the cuprates. According to the spectral-weight distribution near  $E_F$  [Figs. 1(a), 1(c), 1(d), and 1(f)], five main features are labeled as  $\alpha_{1,2}$ ,  $\beta$ , and  $\gamma_{1,2}$ . Their weight distribution is sketched in Fig. 1(b). Note that,  $\alpha_1$  contributes a straight dispersed feature at  $\Gamma$ , thus it could not be recognized from EDCs. The features near  $E_F$  around  $\Gamma$  and  $M$  qualitatively agree with calculations shown in Fig. 1(g). Thus, the spectral weight of  $\alpha_{1,2}$  and  $\gamma_{1,2}$  might be attributed to the hole and electron pockets respectively, as in  $\text{Fe}_{1+y}\text{Te}_x\text{Se}_{1-x}$  [20]. However, contradicting to the calculations, a fair amount of spectral weight around  $X$  could be observed near  $E_F$  in Fig. 1(d), which is an extension of the  $\beta$  feature.

Many changes occur in the SDW state electronic structure (Fig. 2). Most notably, a dramatic reorganization of the spectral weight is observed in Fig. 2(a), where the weight suppression around  $X$  is particularly strong. Such suppression is obvious by comparing the EDCs around  $X$  (thick curves) in Fig. 2(c) and Fig. 1(d). Particularly, sharp quasiparticle peaks appear at  $E_F$  around  $\Gamma$  and  $X$  in Figs. 2(b) and 2(c). The flat quasiparticle dispersion and small weight suggest a very low renormalization factor  $Z$ . Similar to  $\text{BaFe}_2\text{As}_2$ , the SDW state of  $\text{Fe}_{1.06}\text{Te}$  is accompanied by band shifts. As shown by MDCs in Fig. 2(d), the distance between two  $\alpha_2$  peaks decreases in the SDW state, indicating a change of dispersion below  $T_s$ . The  $\gamma_1$  and  $\gamma_2$  bands also exhibit an abrupt momentum shift below  $T_s$ , illustrating the enlargement of the electron pockets and band movement around  $M$  [Fig. 2(e)].

The observed incoherent to coherent lineshape evolution explains the anomalous transport and optical properties of  $\text{Fe}_{1+y}\text{Te}$ , particularly the absence of Drude peak in the paramagnetic state, and insulator-metal transition as shown in Fig. 1(e) [12]. Compared with the incoherent weight distribution of  $\text{Fe}_{1.06}\text{Te}$  in Fig. 2(f), Fig. 2(g) illustrates the well defined band structure of  $\text{Fe}_{1.04}\text{Te}_{0.66}\text{Se}_{0.34}$ , where the SDW is suppressed by the heavy Se doping. Since both systems contain similar amount of interstitial Fe ions, the broad overall lineshape of  $\text{Fe}_{1.06}\text{Te}$  cannot be explained by the magnetic scattering of the excess Fe ions [12]. Furthermore, as illustrated in Fig. 2(h), the quasiparticle width of  $\text{Fe}_{1.06}\text{Te}$  at low temperatures is much sharper than that of  $\text{Fe}_{1.04}\text{Te}_{0.66}\text{Se}_{0.34}$ . This result together with the narrow transitions in resistivity [Fig. 1(e)] and magnetic susceptibility [Fig. 4(d)] confirm the high quality of  $\text{Fe}_{1.06}\text{Te}$  crystals studied here. Therefore, the incoherent lineshape over a large energy scale should be an *intrinsic* property of  $\text{Fe}_{1.06}\text{Te}$ .

Due to the low weight of the coherent quasiparticles, and broad overall lineshape, the dominating effect on the electronic structure is not the band shift but the substantial spectral weight redistribution over a large energy scale. Figure 3(a) plots the difference between the integrated spectral weight over  $[E_F - 0.7 \text{ eV}, E_F + 0.05 \text{ eV}]$  at 135 and 15 K in the Brillouin zone. It is clear

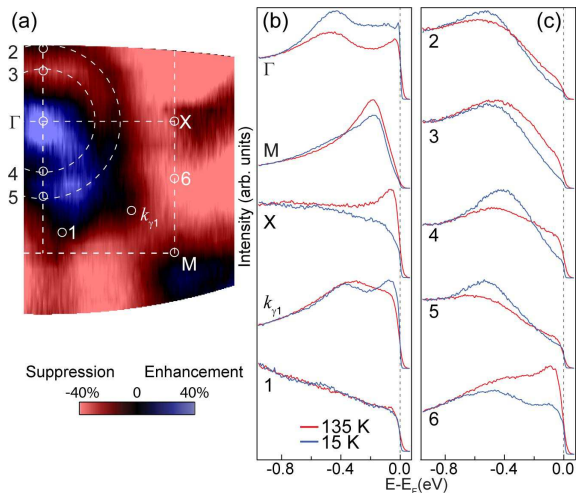


FIG. 3: (Color online) (a) The difference between the integrated spectral weight in 135 K and 15 K over the  $[E_F - 0.7 \text{ eV}, E_F + 0.05 \text{ eV}]$  window for  $\text{Fe}_{1.06}\text{Te}$ . (b) and (c) Temperature dependence of EDCs at various momenta as marked in panel a.

that spectral weight is suppressed over extended momentum region, and enhanced around  $\Gamma$  at low temperature. Figs. 3(b) and 3(c) compare the EDCs at various representative momenta in the paramagnetic and SDW states. The enhancement of spectral weight often happens within  $[E_F - 0.7 \text{ eV}, E_F - 0.2 \text{ eV}]$ , while the suppression often occurs within  $[E_F - 0.4 \text{ eV}, E_F]$ . We note that due to the matrix element effects caused by different polarization, the difference map is not entirely symmetric. For example, the high energy part in EDC at momentum 4 is more prominent than that at momentum 3, although they are symmetric with respect to  $\Gamma$ . Overall, a large amount of spectral weight is transferred from lower binding energies to higher binding energies, as a result, the electronic energy is significantly reduced. Such a suppression over a large energy scale is not relevant to Fermi surface instabilities like nesting. Consistently, no sign of gap opening is observed in all cases of Figs. 3(b) and 3(c). [12, 18]. Early DFT calculations have predicted strong nesting instabilities with incorrect nesting wavevectors along the  $\Gamma - M$  direction [6]. Later on, it has been amended that the excess iron would significantly alter the electronic structure and produce the right wavevector [21, 22]. However, this is ruled out again by the absence of gap observed here.

Detailed temperature evolution of the spectral-weight redistribution near  $T_s$  is shown in Fig. 4. The suppression at  $k_\beta$  occurs abruptly below  $T_s$ , and saturates at low temperatures [Fig. 4(a)]. Furthermore, the temperature cycling experiment with dense steps around  $T_s$  in Fig. 4(b) gives a hysteresis loop in the integrated spectral weight in Fig. 4(c), which almost exactly follows the hysteresis loop in the susceptibility data in Fig. 4(d) of this first order transition. This establishes a direct relation

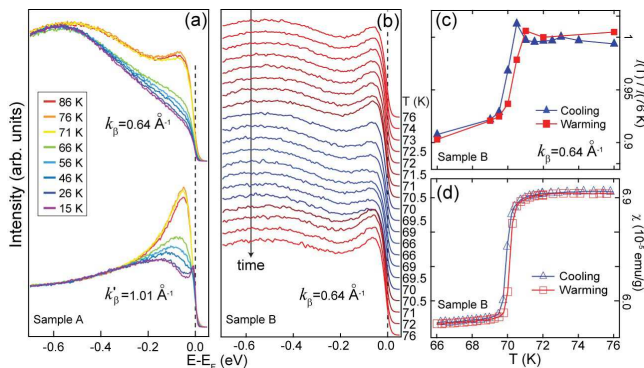


FIG. 4: (Color online) (a) Detailed temperature dependence of EDCs at the Fermi crossings of  $k_{\beta}$  and  $k'_{\beta}$  for sample A. (b) The EDC at  $k_{\beta}$  for sample B in a detailed temperature cycling experiment near  $T_s$ . (c) The integrated spectral weight over  $[E_F - 0.7 \text{ eV}, E_F + 0.05 \text{ eV}]$  as a function of temperature for data in panel b, data are normalized by the integrated weight at 75 K. (d) The magnetic susceptibility hysteresis loop.

between the suppression and the SDW transition, plus proving that our data reflect intrinsic and bulk properties. Similar behavior takes place at  $k'_{\beta}$  [Fig. 4(a)], noting that the difference between  $k_{\beta}$  and  $k'_{\beta}$  might be caused by different  $k_z$ 's or matrix element effects.

Our observation of the intrinsically incoherent electronic structure of  $\text{Fe}_{1.06}\text{Te}$  and the spectral weight redistribution associated with SDW transition suggests strong local magnetic fluctuations and their strong coupling to itinerant electrons. Consequently, carriers are more localized, causing local moments and insulating transport behavior [12], and coherent quasiparticles are destroyed in the paramagnetic states. However in the SDW state, when the spin fluctuations are suppressed due to the opening of a spin gap as demonstrated by inelastic neutron scattering [24], the sharp quasiparticles emerge. Consistently, it is found that the ordered moment in  $\text{FeTe}$  is about  $2 \mu_B$  [11], much larger than the  $0.87 \mu_B$  in  $\text{BaFe}_2\text{As}_2$ , or the  $0.36 \mu_B$  in  $\text{LaOFeAs}$  [8, 9]. Theoretically, the models based on magnetic exchange interactions between the nearest and next-nearest neighbor iron moments have successfully explained the bicollinear magnetic structure in  $\text{Fe}_{1+y}\text{Te}$  [25, 26]. Our data will be a

decisive support, if incoherent electronic structure and related spectral weight redistribution can be reproduced in these models.

Furthermore, an early ARPES experiment [18] has shown that  $\text{Fe}_{1.05}\text{Te}$  ( $T_s = 65 \text{ K}$ ) exhibits an electronic structure close to that of the non-magnetic  $\text{Fe}_{1.04}\text{Te}_{0.66}\text{Se}_{0.34}$  [20], with more coherent electronic structure. Since the magnetic order in iron chalcogenides could be strongly suppressed by just a small amount of Se, excess iron, or pressure [13, 27, 28], our samples with higher  $T_s$  of 70 K are in a more strongly ordered state. It is remarkable to observe that the strong correlation effect is enhanced so dramatically here, while  $T_s$  is just slightly increased. It is sensible to study how the correlations in iron-based systems are affected by anions (P/As/Se/Te), doping, and pressure.

Similar behavior has been observed in charge density wave (CDW) systems like  $2\text{H-TaS}_2$ , where strong electron-phonon interactions cause incoherent polaronic spectral lineshape, and spectral weight at the  $E_F$  over the entire Brillouin zone. It was found that the massive spectral-weight suppression over a large momentum and energy phase space, instead of Fermi surface nesting, is responsible for the CDW in  $2\text{H-TaS}_2$  and  $2\text{H-NbSe}_2$  [29, 30]. The analogous mechanism of SDW found here for  $\text{Fe}_{1.06}\text{Te}$  indicates the density waves at the strong coupling limit share a universal theme, which makes them fundamentally different from the weak interaction systems.

To summarize, we have carried out a systematic photoemission investigation of high quality  $\alpha\text{-Fe}_{1.06}\text{Te}$  single crystals. We observed an intrinsically incoherent electronic structure, and massive spectral weight redistribution that is responsible for the SDW transition. Our results demonstrate that correlations are probably the strongest in  $\text{Fe}_{1+y}\text{Te}$  among all Fe-HTSCs and their parent compounds discovered so far, and reveal universal behaviors of density waves in the presence of strong interactions.

We thank Dr. Donghui Lu for helpful discussions. This work was supported by the NSFC, MOE, MOST (National Basic Research Program No. 2006CB921300), and STCSM of China.

[1] Y. Kamihara *et al.*, *J. Am. Chem. Soc.* **130**, 3296 (2008).  
 [2] X. H. Chen *et al.*, *Nature (London)* **453**, 761 (2008).  
 [3] M. Rottor *et al.*, *Phys. Rev. Lett.* **101**, 107006 (2008).  
 [4] K. W. Yeh *et al.*, *Europhys. Lett.* **84**, 37002 (2008).  
 [5] S. Margadonna *et al.*, *Phys. Rev. B* **80**, 064506 (2009).  
 [6] A. Subedi *et al.*, *Phys. Rev. B* **78**, 134514 (2008).  
 [7] D. J. Singh, *Phys. Rev. B* **78**, 134514 (2008).  
 [8] C. de la Cruz *et al.*, *Nature* **453**, 899 (2008).  
 [9] Q. Huang *et al.*, *Phys. Rev. Lett.* **101**, 257003 (2008).  
 [10] W. Bao *et al.*, *Phys. Rev. Lett.* **102**, 247001 (2009).

[11] S. L. Li *et al.*, *Phys. Rev. B* **79**, 054503 (2009).  
 [12] G. F. Chen *et al.*, *Phys. Rev. B* **79**, 140509 (2009).  
 [13] T. J. Liu *et al.*, *Phys. Rev. B* **80**, 174509 (2009).  
 [14] L. X. Yang *et al.*, *Phys. Rev. Lett.* **102**, 107002 (2009).  
 [15] Y. Zhang *et al.*, *Phys. Rev. Lett.* **102**, 127003 (2009).  
 [16] M. Yi *et al.*, *Phys. Rev. B* **80**, 174510 (2009).  
 [17] J. Dong *et al.*, *Europhys. Lett.* **83**, 27006 (2008).  
 [18] Y. Xia *et al.*, *Phys. Rev. Lett.* **103**, 037002 (2009).  
 [19] T. Taen *et al.*, Arxiv: 0906.1951 [cond-mat.str-el]. (2009).  
 [20] F. Chen *et al.*, *Phys. Rev. B* **81**, 014526 (2010).

- [21] L. Zhang, D. J. Singh, and M. H. Du, Phys. Rev. B **79**, 134514 (2008).
- [22] M. J. Han and S. Y. Savrasov, Phys. Rev. Lett. **103**, 067001 (2009).
- [23] A. Tamai *et al.*, Arxiv: 0912.3152 [cond-mat.str-el].
- [24] J. Zhao *et al.*, Phys. Rev. Lett. **101**, 167203 (2008).
- [25] C. Fang, B. Andrei Bernevig and J. P. Hu, Europhys. Lett. **86**, 67005 (2009).
- [26] F. J. Ma *et al.*, Phys. Rev. Lett. **102**, 177003 (2009).
- [27] H. Okada *et al.*, J. Phys. Soc. Jpn. **78**, 083709 (2009).
- [28] P. L. Paulose, C. S. Yadav, and K. M. Subhedar, Arxiv: 0907.3513 [cond-mat.super-con].
- [29] D. W. Shen *et al.*, Phys. Rev. Lett. **99**, 216404 (2007).
- [30] D. W. Shen *et al.*, Phys. Rev. Lett. **101**, 226406 (2008).